Sigma J Eng & Nat Sci 38 (1), 2020, 213-226

Sigma Journal of Engineering and Natural Sciences
Sigma Mühendislik ve Fen Bilimleri Dergisi

Research Article

EFFECT OF THE VARIABLE RESISTANCE ROTOR SLOT DESIGN ON THE PERFORMANCE OF THE SINGLE PHASE ASYNCHRONOUS MOTOR (SPAM)

Merve ŞEN KURT*[1], Ahmet FENERCİOĞLU[2]

[1]*Amasya University, Dept. of Electrical and Electronics Eng., AMASYA;* ORCID: 0000-0003-1648-9368
[2]*Tokat Gaziosmanpaşa University, Dept. of Mechatronics Eng., TOKAT;* ORCID: 0000-0002-1522-6868

Received: 22.02.2019 Revised: 25.10.2019 Accepted: 04.12.2019

ABSTRACT

In this study, the effect of the rotor slot depth of the single-phase asynchronous motor (SPAM) on the output performance was examined. Single-phase and two-pole squirrel cage asynchronous motor with run capacitor that has 96 W output power was used in analysis. SPAMs having Nema B class rotor which have variable resistance rotor slot structure, starting and steady-state operation were analyzed by 2D finite element method. The rotor bar cross sectional area and the rotor bar materials were taken as the same, and the rotor slot depth (H_{s2}) parameter was changed. Rotor slot structures having different depth were obtained by changing the H_{s2} in the range of 3-7 mm with steps of 0.25 mm. Performance variables according to different rotor slot depths were comparatively examined as speed (n), input-output powers (P_i-P_o), efficiency (η), current (I), torque (T), and power factor (PF). The magnetic flux densities (B), flux lines and current densities in the rotor bars (J) at the stator and rotor were visually presented. The Nema B class motor with the best performance values for all parameters was determined as the best model. In this model, the average speed, power factor and efficiency are 2954 rpm, 0.9 and 68.9%, respectively in steady-state operation. Magnetic flux densities (B), flux lines and current densities in rotor bars (J) at different points of the stator and rotor were examined and it was observed that they did not exceed the limit values defined in the literature.
Keywords: Single phase asynchronous motor, finite element method, variable resistance rotor slot, slot depth of rotor.

1. INTRODUCTION

It is known that SPAMs have superior properties because they are powered on single-phase grid and have low costs and simple structures. Furthermore, the fact that SPAM does not have a rotating magnetic field is known as its major disadvantage. Since a rotating stator magnetic field is not formed, single-phase asynchronous motors cannot start by themselves.

It is expected that whereas a high-performance asynchronous motor has a high starting torque and low current at the starting time, it has a low rated slip and high efficiency in steady-state operation [1]. The most basic way of achieving this is to design two parallel bars (top bar with a high rotor resistance and reactance, and the bottom bar with a lower rotor resistance and reactance) in which the rotor current can flow. While most of the current prefer the high

* Corresponding Author: e-mail: merve.sen@amasya.edu.tr, tel: (358) 260 00 60

resistance path due to the skin effect when the frequency of the rotor is relatively high at the starting time, they pass through the low resistanc e section during the steady-state operation. Thus, thanks to the two different rotor bar, while starting current is limited due to the high resistance effect of the rotor at the starting time, the decreasing of motor efficiency is prevented by the low resistance effect of the rotor during the steady-state operation. By using a deep slot or double cage rotor slot structure, the rotor resistance can be ensured to be variable.

A few studies examining the effect of variable resistance rotor slot design on motor performance using deep slot or double cage rotor slot structure are given below.

In the study given in [2], the effect of rotor and stator slot geometric sizes on the performance characteristics of a squirrel cage induction motor was investigated. The average torque, output power, efficiency increases and torque fluctuation, power losses decreases with the selection of the optimal value of the rotor slot depth, which is one of the geometric sizes considered. It is concluded that squirrel cage induction motor has good working performance with the selection of the optimal value of the rotor slot depth.

In their analysis study, Akhtar et al. [3] concluded that the rotor slot structure significantly affected the asynchronous motor performance. According to their study, while short and wide rotor slots should be preferred in applications where locked rotor torque is important, deep and wide rotor slot types should be preferred in applications where high efficiency is desired. In addition, it was also observed in this study that when all parameters were constant, by using of narrower and higher slot type, the efficiency increased but the power factor decreased.

Yoshino et al. [4] presented 2 different double cage rotor slot models for a squirrel cage induction motor. The rotor slot structure of the first model consists of 2 parts, the upper part of which is rectangular and the lower part which is deep slot. The second model consists of 3 pieces, the top of which is 2 rounds and the bottom of which is deep slot. In both models, the deep slot rotor part has lower electrical resistance and the upper parts have higher electrical resistance. Therefore, in starting operation, the majority of the current flows from the upper part of the rotor due to the reactance distribution at high frequency, in normal operation with lower frequency, the rotor flows through the deep slot forming the bottom of the slot. Both rotor slot models designed increase the locked rotor torque of a high efficiency asynchronous motor in rated operating condition.

In a study in the literature, the advantages of asynchronous motors with double cage rotor slot structure over asynchronous motors with single cage rotor slot structure are presented. The author et al. examined the torque-speed and stator current-speed characteristics of asynchronous motors with single and double cage rotors using Matlab software. As a result of the study, in applications where the starting torque is important, the use of a double cage rotor slot can be preferred because of increasing the starting torque and decreasing the starting current [5].

Iqbal and Singh [6], have compared recent studies related to the effect of the rotor slot geometry on the performance of the asynchronous motor. As a result of the studies discussed, the rotor slot depth, width, slot shape, rotor slot number, rotor core material, rotor winding, rotor slot opening which forms the rotor slot geometry has a significant effect on the performance of the induction motor.

In this study, the rotor slot depth (H_{s2}) of SPAM with single-phase, two-pole and run capacitor that has 96 W output power was changed in the range of 3-7 mm with steps of 0.25 mm and as a result, different rotor slot models were obtained. The rotor bar areas and the rotor bar materials of all models were bought as the same. The model having the best performance was determined by taking into account the performance variables (speed, input-output power, efficiency, current, torque, power factor) of models with different rotor slot depths. The requirement to remain within the range of values permitted in literature was examined by controlling the values of the flux densities in stator-rotor cores and the values of the current densities in rotor bars of the model with best performance.

2. MATERIAL AND METH OD

In the design of the variable resistance rotor bar , in order to benefit from the skin effect, the smallest value that the sloth depth (δ) can take is calculated by using Equation (1).

$$\delta = \sqrt{\frac{\rho_{br}}{\mu_0 \pi f}} \tag{1}$$

In this equation, δ, ρ_{br} , f and μ_0 refer to the least skin effect depth that it should be, specific resistance (Ω.m), frequency (Hz), and magnetic permeability of the cavity (H/m), respectively [7].

The test motor in NEMA B deep slot class category used in this study was numerically modeled with FEM method by using the Ansys/Maxwell software. Then, in order to improve the motor performance, rotor slot models with different depths were obtained by changing the rotor slot depth (H_{s2}) in 3-7 mm with 0.25 mm steps. In all designed models, the total rotor slot area was kept constant in order to keep the current density passing through the rotor bars constant. The keeping of the rotor slot area constant in all models ensured that production costs were the same. As a result of the electromagnetic analysis, the model with deep slot and having the best performance values was determined as the best model.

2.1. Mathematical Approximation

It is known that rotor bar resistance and rotor bar inductance are the leading parameters determining the motor performance in single-phase asynchronous motors. For the motor having deep slot structure, the rotor bar resistance (R_{br}) is obtained by using Eq. (2).

$$R_{br} = \rho_{br} \frac{l_{br}}{A_{br}} \tag{2}$$

In this equation, ρ_{br} refers to the rotor bar specific resistance which is the inherent property of the rotor bar. In the same equation, l_{br} and A_{br} are defined as to the rotor bar length and rotor bar area, respectively [8]. l_{br} which is placed in the rotor slots by different methods and refers to the length of the rotor bars is a magnitude that directly changes with the depth of the rotor slot.

The rotor bar inductance (L_b) is another important parameter for determining the motor performance is expressed by Eq.(3).

$$L_b = \mu_0 . l_{br} . N_r^2 . \lambda_b \tag{3}$$

In this equation, μ_0 refers to the magnetic permeability of the airgap. In the same equation, *Nr and* λ_b are defined as to the number of rotor slots and the rotor bar permeability coefficient, respectively.

The rotor bar permeability coefficient (λb) is a magnitude that varies depending on the geometry of the rotor slot. In the literature, detailed calculations in order to determinate to λb for different motor classes in [8,9].

Rotor slot pitch (τr) which depends on the size of the external radius of the rotor (Dor) and the number of rotor slot (Nr) varies with Eq. (4).

$$\tau_r = \frac{2\pi \times D_{or}}{N_r} = \frac{2\pi \times 30.22}{30} = 6.326 \times 10^{-3}\ \text{m} \tag{4}$$

In single-phase asynchronous motors, the rotor tooth width (b_{tr}) is accepted approximately 0.3 ratio of the rotor slot pitch (τ_r) [8].

$$b_{tr} = \tau_r \times 0.3 = 1.898 \times 10^{-3}\text{m} \tag{5}$$

Rotor slot bottom width (B_{s1}) is calculated by using Eq. (6).

$$B_{s1} = \tau_r - b_{tr} = (6.326 - 1.898) \times 10^{-3} = 4.428 \times 10^{-3}\ \text{m} \tag{6}$$

In this study, NEMA class B rotor slot structure is investigated, the permeability coefficient (λ_b) is calculated by using Eq. (7).

$$\lambda_b = \frac{H_{s2}}{3B_{s1}}\mathrm{k}_1 + \mathrm{k}_2 - \frac{\mathrm{h_{or}}}{2B_{s1}} + \frac{\mathrm{h_{or}}}{B_{s0}} \quad (7)$$

In Eq. (7), k_2 refers to deep slot constant that varies between 0.645 and 0.785 in the literature. And k_1 (k_1<1) refers to the inductance attenuation factor. The geometric dimensions of the rotor slot in the equation are described in Table 1. As seen in Equation 7, the permeability coefficient is a magnitude that changes depending on the slot depth (H_{s2}) parameter. The decrease on slot depth contributes to the decrease on permeability coefficient and thereby decrease on value of the leakage inductance.

2.2. Finite Element Method (FEM)

The finite element model of the test motor that used in this study was created by using the Ansys/Maxwell software. This analysis provides high precision solutions. This software created a mesh structure consisting of finite small elements of designed SPAM's geometry to achieve the numerical solution with FEM. Figure 1 (a) shows the mesh view of the stator core and the stator windings, Figure 1 (b) shows the mesh view of the rotor core and the rotor bars, respectively.

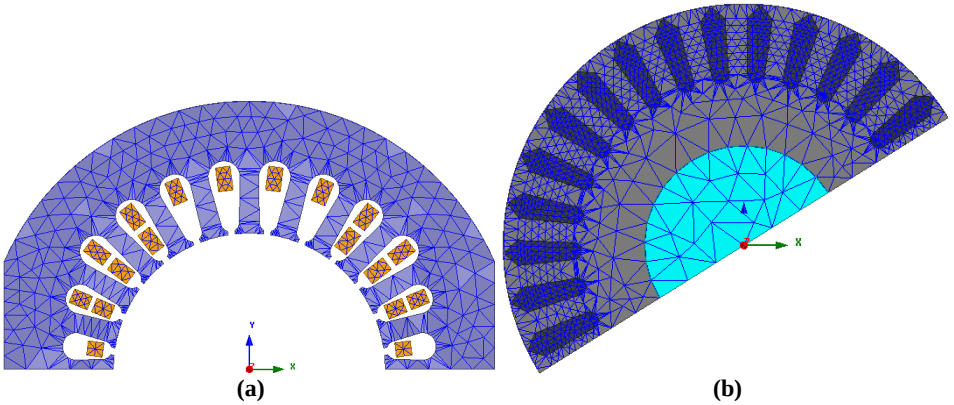

Figure 1. (a) The stator core and the stator windings, (b) The rotor core and the rotor bars

2.3. Model of SPAM

A SPAM with squirrel cage rotor has 96 W output power, 2950 rpm shaft speed and 0.31 Nm load torque, respectively. Main and auxiliary windings were placed into 24 slots in stator core. In order to reduce eddy current losses, the stator and rotor cores were manufactured from laminated steel with a 0.95 stacking factor. The analyses were carried out on the half-model by taking advantage of the symmetrical feature of SPAM which was discussed in the scope of the study. Figure 2 shows the analysis model of the motor.

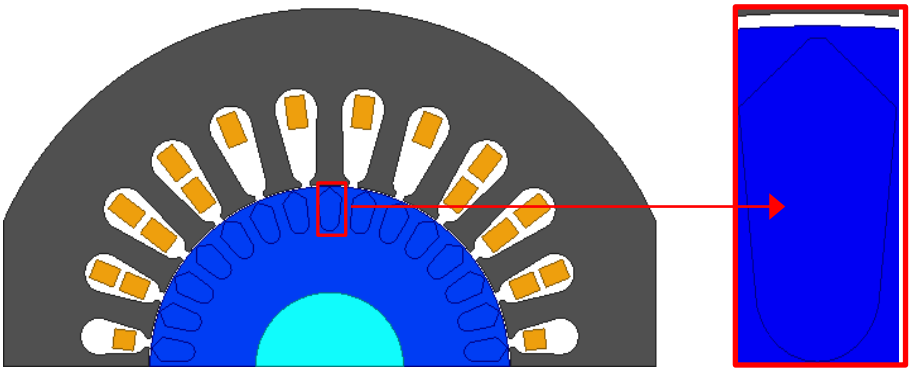

Figure 2. Deep slot model of SPAM

The SPAM consists of 30 rotor bars that are described as "tapered rotor slot model" and whose lower edge are rounded, and the upper edge are triangular. The symbols of the parameters forming the tapered rotor slot geometry of the motor are presented in Table 1.

Table 1. The rotor slot geometric dimensions of the SPAM

Symbol	Explanations
H_{s2}	Rotor slot height/depth
B_{s1}	Rotor slot top width
B_{s2}	Rotor slot bottom width
B_{s0}	Rotor slot opening width
h_{or}	Rotor slot opening height
H_{s0}	Rotor slot-core height
A_r	Rotor slot area

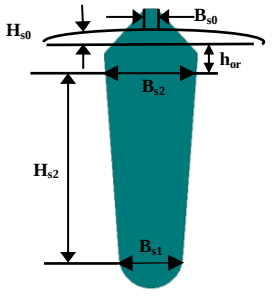

Two-dimensional finite element analyses of the models with rotor slots in different depths and having same rotor slot areas (A_r = 21.85 mm^2) were performed. In the analyses, slot depth (H_{s2}) was changed between 3≤ H_{s2} ≤7mm with 0.25 mm steps and through this way, rotor slot models with different depth were obtained (Figure 3).

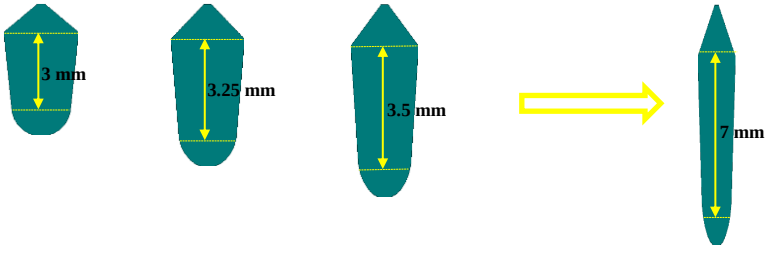

Figure 3. Demonstration of models having different rotor slot depths

Although the B_{s0}, H_{s01} and H_{s0} parameters of the examined models were equal, lower and upper widths (B_{s1}, B_{s2}) of the slot were changed in order to keep the slot areas equal at different slot depths. In these changes, it was paid attention the slot teeth to remain in parallel structure. As a result of the analyses, both the electrical and magnetic investigations of the models were performed and the optimal rotor model with deep slot was determined.

2.4. The starting circuit of SPAM

The starting circuit of the motor taken in the scope of the study is shown in Figure 4.

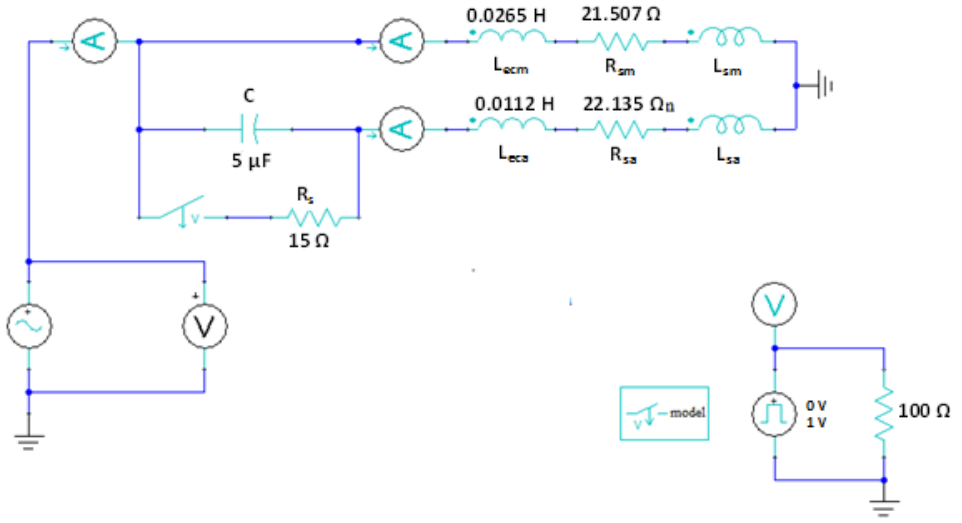

Figure 4. Starting circuit of SPAM

The parallel connected horizontal branches in starting circuit show the main and auxiliary winding, respectively. R_{sm}, L_{ecm} and L_{sm} refer to main winding resistance, main end-winding inductance and main winding phase inductance, respectively. R_{sa}, L_{eca}, L_{sa} also refer to auxiliary winding resistance, auxiliary end-winding inductance and phase inductance of auxiliary winding, respectively. Phase inductances vary depending on the magnetic flux. Permanent capacitor (C) connected serially to the auxiliary winding and the starting resistance (R_s) connected parallel to this are shown. In the case of the starting of the motor with a run capacitor, the starting resistance connected parallel to capacitor is activated with a switch. When the motor reaches 2800 rpm after starting, the starting resistance (R_s) is deactivated by means of this switch and the auxiliary winding remains active continuously through the capacitor.

3. RESULTS AND DISCUSSIONS

3.1. The Results of the Analysis

In the analyses, the effect of the slot depth increasing on the output performance were observed. Performance variables of such as speed, electromagnetic torque, stator current, power factor, input-output power and efficiency are taken into consideration. There is no significant change in the speed. There is a very small increase of 0.09% (about 3 rpm) between the highest and lowest speed values.

Considering all slot depths, the average value of electromagnetic torque is considered as approximately 0.33 Nm due to the small difference it is negligible. Because there is no significant change in torque and speed with respect to the slot depth. Therefore the output power of the motor can be accepted approximately constant.

The increase in the slot depth changes the magnetic reluctance accordance with length of the magnetic flux path and cross section. This change causes a change in the current and power factor of the one phase stator because of influencing the inductance. Figure 5 shows the change in the current drawn from the source depending on the increase in the rotor slot depth.

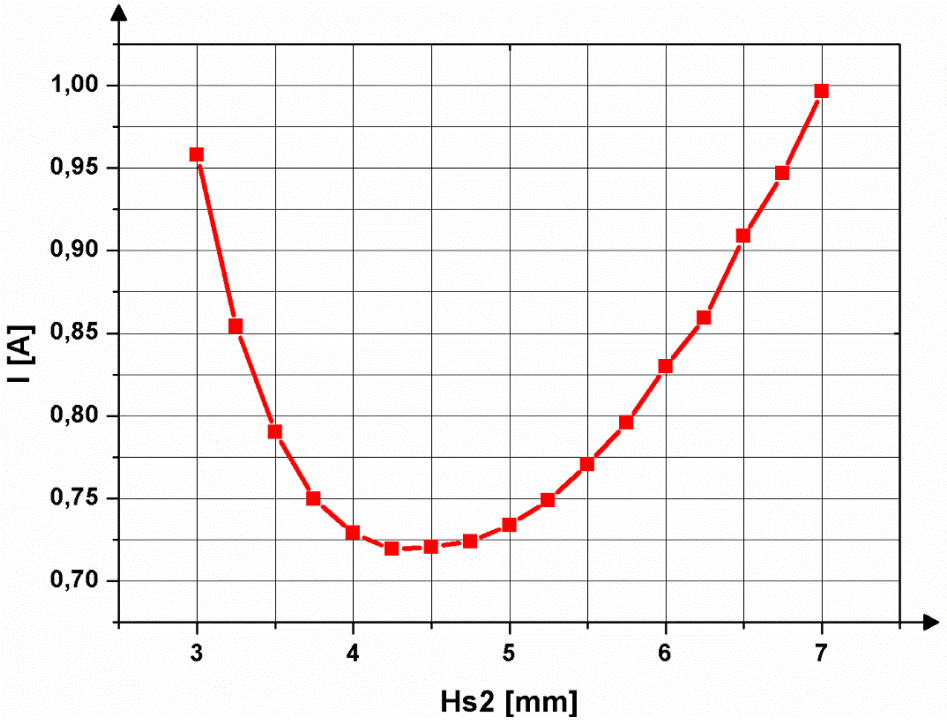

Figure 5. Variation of current depending on rotor slot depth

As seen in Figure 5, the current gradually decreased depending on increase in the depth, and after taking the value of 0.7192 A, which is the smallest value in H_{s2} = 4.25 mm value, it gradually increased, and at the value of H_{s2}=7 mm, it reached to value of I = 0.996 A.

The starting current according to the rotor slot depth is approximately 10.3 A and there is no significant change in the starting current according to the change of H_{s2}. And the motor reaches steady state after 0.55 s for all of the rotor slot depths.

Figure 6 shows the power factor change depending on rotor slot depth.

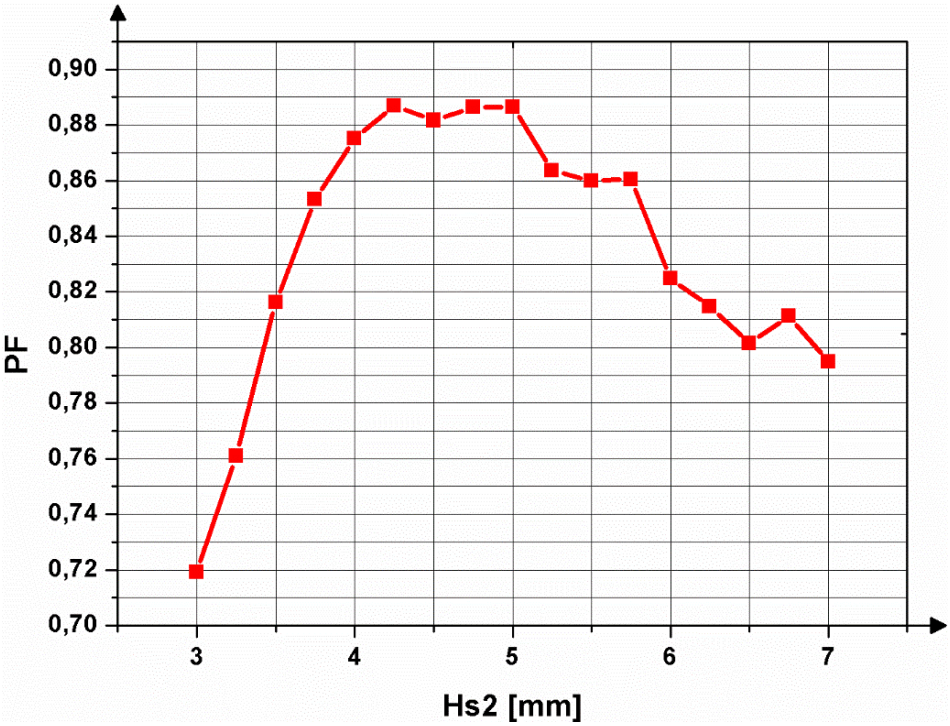

Figure 6. Variation of PF depending on rotor slot depth

As seen in Figure 6, the power factor takes values between 0.7- 0.9. When the depth is increased from H_{s2} = 3 mm, the PF gradually increases; after taking the value of 0.9, which is the highest value, in the range of H_{s2}=3.75-4.75, it drops to 0.8 in the range of H_{s2}= 6-7 mm. When the PF is considered as the performance variable, it should be selected in the range of H_{s2}=3.75-4.75.

Table 2 shows the input/output power, efficiency and power factor variations of the motor in steady-state time depending on the increase in rotor slot depth. It is observed that motor efficiency increases between the height of the slot ($H_{s2)}$ from 3 mm up to 4 mm, it remains approximately constant between 3.75 and 4.75 mm and it decreases after 5 mm.

Table 2. Input/output power and efficiency values depending on rotor slot depth

Rotor slot depth H_{s2} *(mm)*	*Input power,* P_i *(W)*	*Output power,* P_o *(W)*	*Efficiency,* η *(%)*
3.0	151.613	95.641	63.082
3.25	142.997	96.189	67.266
3.5	141.909	96.144	67.751
3.75	140.777	95.912	68.130
4.0	**140.398**	**96.738**	**68.902**
4.25	140.338	95.824	68.281
4.5	139.826	96.315	68.882
4.75	141.199	96.257	68.171
5.0	143.100	95.915	67.027
5.25	142.321	95.855	67.351
5.5	145.777	96.855	66.440
5.75	150.681	96.327	63.928
6.0	150.614	96.044	63.768
6.25	153.991	94.149	61.139
6.5	160.256	96.080	59.954
6.75	168.987	96.127	56.884
7.0	174.271	96.261	55.236

When the electrical and mechanical parameters were considered, the optimum rotor slot depth was determined as H_{s2} =4 mm. After selecting the optimal rotor slot geometry, magnetic flux density values in the regions of the stator yoke, stator teeth, rotor yoke, rotor teeth were examined. After the model with the optimal rotor slot geometry is selected considering the electrical and mechanical parameters, it should be paid attention the requirement that the magnetic flux density in the stator, rotor teeth and yoke does not exceed the limit values permitted in the literature. In the literature, the maximum values of magnetic flux density were defined by Lipo [2004] as 1.7 T in stator yoke, 2.1 T in stator teeth, 1.7 T in rotor yoke and 2.2 T in rotor teeths [10]

Figure 7 shows the vectorial (Figure 7 (a)) and scalar (Figure 7 (b)) distributions of the magnetic flux density of the stator and rotor cores of the model with the optimal rotor slot depth.

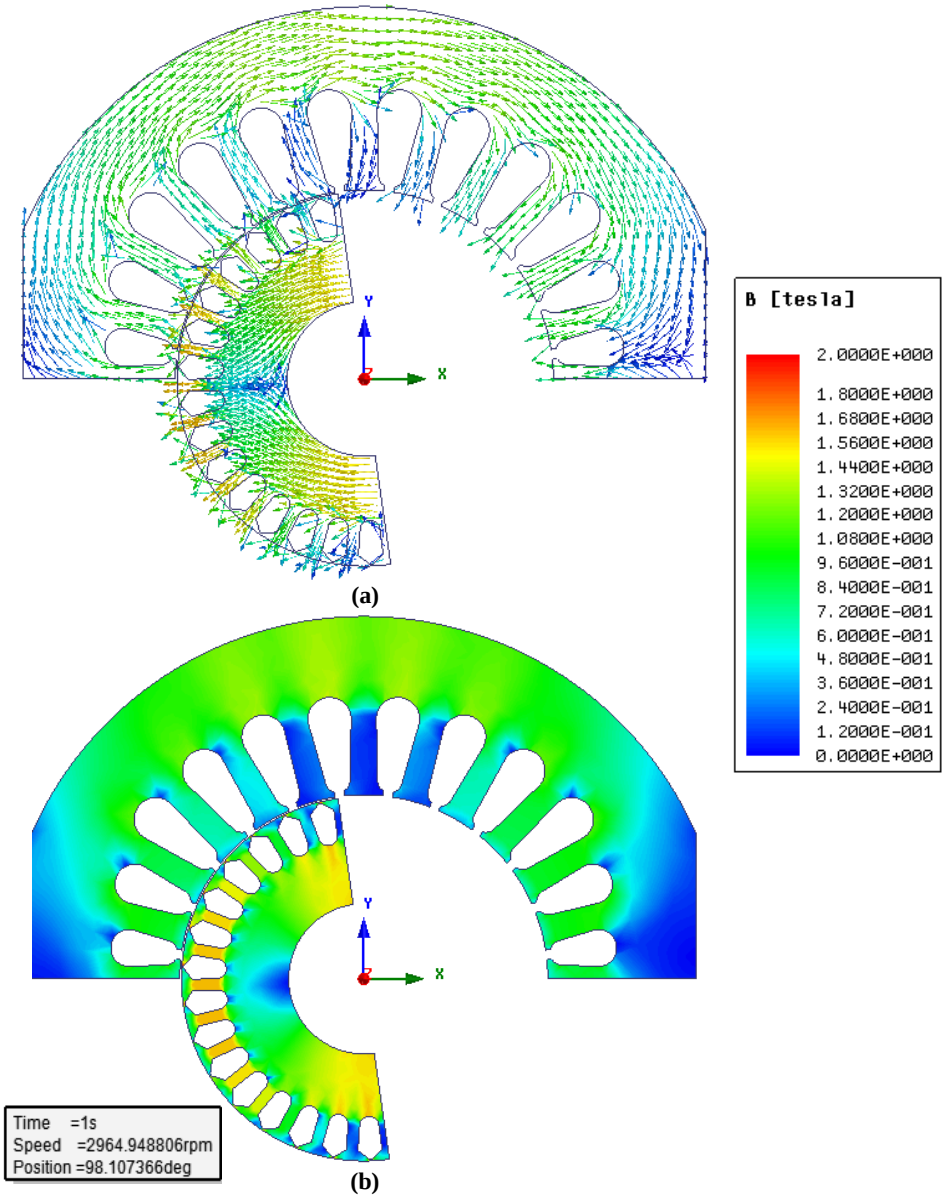

Figure 7. Magnetic flux distribution of the model with optimal rotor slot depth with transient analysis (a) vectorial, (b) scalar

When the maximum values of the magnetic flux density in the various regions of stator and rotor cores of the model with optimum rotor slot depth were examined, it was observed as 1.36 T in the stator yoke region, 1.04 T in the stator teeth region, 1.58 T in the rotor yoke region, and 1.61 T in the rotor teeth region. Based on the results obtained, it was concluded that the magnetic

flux density in various regions of the stator and rotor did not exceed the limit values specified by Lipo (2004). When selecting the optimal rotor slot geometry, the rotor bar current density (J) as well as the electrical performance variables and the core magnetic flux density (B) should also be considered. The rotor current density of the model in the steady state is given in Figure 8.

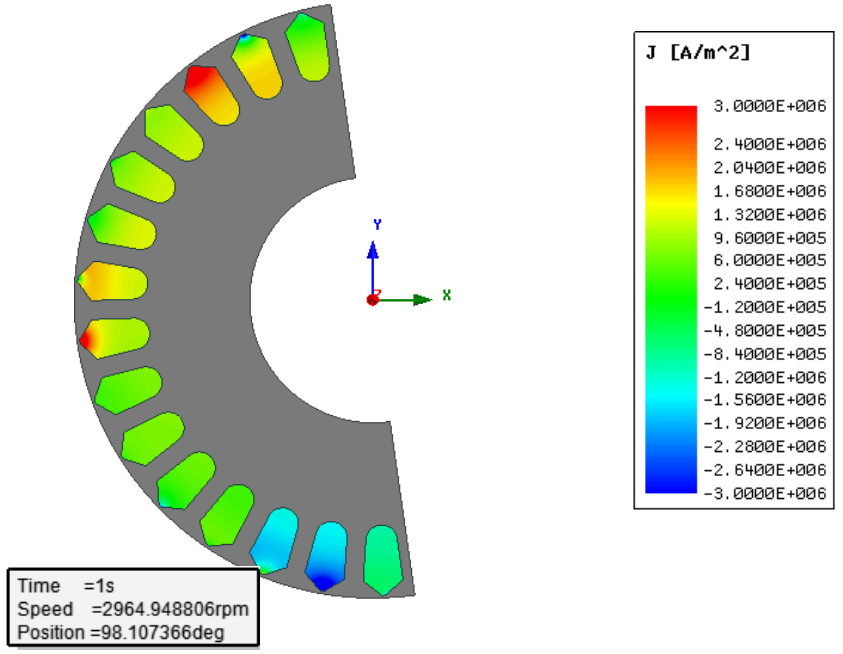

Figure 8. Distribution of current density passing through the rotor bars of the model having optimal rotor slot depth

The current density in rotor bars (Jb) must be in the range of 2.2 < Jb< 4.5 A/mm2 in small motors having aluminum rotor bars [11]. Considering the current density of the rotor bars of the designed model, it is observed that the permissible limits are not exceeded (Figure 8).

Figure 9 shows the time-dependent variation of the speed for the models having different rotor slot depths. As it can be seen in Figure 9, the shaft speed of motor reaches steady-state to the smallest time (t=0.56 s) for H_{s2}= 3 mm. And it reaches steady-state to the longest time (t=0.67 s) for H_{s2}= 6.25 mm.

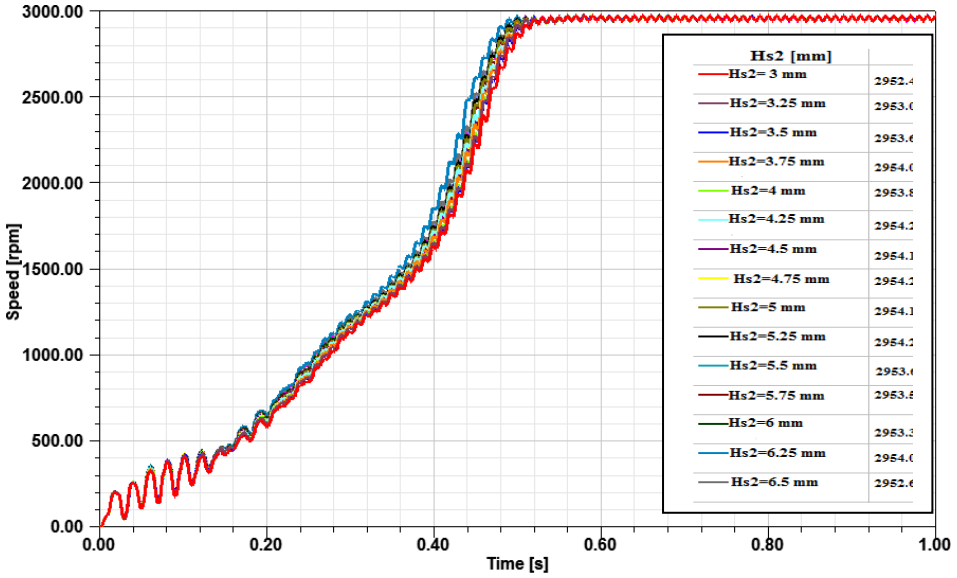

Figure 9. Time-dependent variation of the speed in different rotor slot depths

It is known that depending on the skin effect, most of the current prefer the path with high resistance at the starting time when the rotor frequency is relatively high. The top surface areas and geometries of bar that are active at the start time have the same properties in all models. Therefore, it is concluded that the time dependent curves times of the motors to reach the steady state are in very close values to each other.

4. RESULTS

In this study, a SPAM that has run capacitor having label values of 96 W output power and has NEMA B class rotor slot structure was used as the test motor. It was aimed to improve the output parameters by changing the rotor slot depth in order to increase the efficiency and performance of the motor. For this purpose, 2-dimensional analyses were performed by changing the depth of the slot (H_{s2}) in the range of 3-7 mm with 0.25 mm steps. In these analyses, while all motor parameters were constant, the effect of the rotor slot depth on the electrical and mechanical performance and efficiency of the motor was examined.

There is no significant difference between the speed values due to the increase in rotor slot depth. The average value of the load torque is approximately 0,312 Nm for all of the rotor slot depths. The power factor takes values between 0.7- 0.9 for different rotor slot depths. Motor efficiency increases due to changes in input and output powers for rotor slot depth between 3-4 mm. When the rotor slot depth is bigger than 4 mm, motor efficiency decreases. When the electrical and mechanical parameters are considered, the optimal rotor slot depth is determined as H_{s2} = 4 mm.

According to the results of the analysis for the transient and steady state conditions, the values in which each variable was the best in terms of performance parameters were determined. The geometric dimensions of the rotor slot for H_{s2} = 4 mm where the best performance data were obtained are given in Table 3.

Table 3. The rotor slot geometric dimensions for H_{s2}=4 mm

Symbol	***Quantity***	***Size***	
H_{s2}	Rotor slot height/depth	4 mm	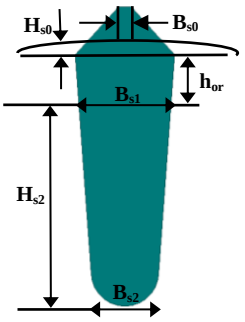
B_{s1}	Rotor slot top width	3.67 mm	
B_{s2}	Rotor slot bottom width	2.96 mm	
B_{s0}	Rotor slot opening height	1 mm	
h_{or}	Rotor slot opening height	1.525 mm	
H_{s0}	Rotor slot-core height	0.2 m	
A_r	Rotor slot area	21.856 mm^2	

The electrical and mechanical parameter values in steady state for H_{s2}=4 mm are shown in Table 4.

Tablo 4. Performance data for H_{s2}=4 mm

Parameter	***H_{s2} (4 mm)***
Starting Time	0.5 sec
Rated Speed	2954 rpm
Phase current	0.729 A
Electromagnetic Torque	0.331 Nm
Load Torque	0.313 Nm
Power Factor (PF)	0.875
Input Power	140.4 W
Output Power	96.7 W
Efficiency	%68.9

In the current studies proposed in the literature, electrical and mechanical performance values are considered when choosing the optimal model for an SPAM. In this study current density on bars and distribution of the magnetic field density on stator and rotor cores density have to take into consideration besides electrical performance variables when an optimal slot geometry is chosen.

In this study, it was concluded that after the model selection with the best rotor slot height and after the proceeding of the designed motor to the steady state, the maximum values of the magnetic flux density in the region of the stator, rotor yoke and teeth, and the current density in the rotor did not exceed limit values permitted in the literature.

Another original aspect of this study, rotor bar areas and rotor bar materials were kept constant in all models so that the current density passing through the rotor bars was the same value.

REFERENCES

[1] Şal S., İmeryüz M. and Ergene L. T., (2012) Kafesli Asenkron Motorlarda Maliyet Kısıtı Altında Rotor Çubuklarının Analizi, *EMO Bilimsel Dergi* 3, 23-28.

[2] Gundogdu T., Zhu Z., Mipo J. C. and Personnaz S., (2019) Influence of Stator and Rotor Geometric Parameters on Rotor Bar Current Waveform and Performance of Ims, *The Journal of Engineering* 6, 3649-3654.

[3] Akhtar M. J., Behera R. K. and Parida S. K., (2014) Optimized Rotor Slot Shape for Squirrel Cage Induction Motor in Electric Propulsion Application, *6th India International Conference on Power Electronics*, IICPE, 8-10 December, Kurukshetra, India.

[4] Yoshino H., Yabe K., Baba K., Oikawa T. and Tsutsumi T., (2012) United States Patent No. *US 8,319,388 B2*.

[5] Yahaya E. A., Omokhafe T., Agbachi E. O. and James A. G., (2015) Advantage of Double Cage Rotor over Single Cage Rotor Induction Motor, *International Journal of Innovative Systems Design and Engineering* 6, 1-4.

[6] Iqbal M. A. and Singh G., (2014) A Review on Influence of Rotor Geometry on the Performance of Single-Phase Capacitor-Run Induction Motor, *International Journal of Advanced Research in Electrical, Electronics and Instrumentation Engineering* 3, 10216-10224.

[7] Fireteanu V., Tudorache T. and Turcanu O. A., (2007) Optimal Design of Rotor Slot Geometry of Squirrel-Cage Type Induction Motors, *IEEE International Conference on Electric Machines & Drives*, IEMDC, 3-5 May, Antalya, Turkey.

[8] Sadarangani C., (2000) Electric Machines Design and Analysis of Induction and Permanent Magnet Motors, *Royal Institute of Technology*, Stockholm, Sweeden.

[9] Boldea I. and Nasar S. A., (2010) The Induction Machines Design Handbook, *CRC Press*, US.

[10] Pyronen J., Jokinen T., (2008) Design of Rotating Electrical Machines, *John Wiley & Sons*, West Sussex, United Kingdom.

[11] Lipo T. A., (2004) Introduction to AC Machine Design, *Wiley IEEE Express*, New Jersey, US.

[12] Fu F. and Tang X., (2002) Induction Machine Design Handbook, *China Machine Press*, China.